Catal Lett (2012) 142:112–117
DOI 10.1007/s10562-011-0736-6

Enhanced Concentration of Medium Strength Brönsted Acid Sites in Aluminium-Modified β Zeolite

Dolores Esquivel · Aurora J. Cruz-Cabeza · César Jiménez-Sanchidrián · Francisco J. Romero-Salguero

Received: 5 October 2011 / Accepted: 2 November 2011 / Published online: 12 November 2011

Abstract A beta zeolite modified by treatment with aluminium ions has been characterized by different techniques, such as XRD, XPS, N_2 adsorption, and TPD of pyridine and acetonitrile. Compared to the parent zeolite, it has shown some differences concerning the local environment of the aluminium atoms and the distribution of the acid sites. The modified zeolite has been tested as catalyst in a model reaction, i.e. the conversion of methanol to hydrocarbons, where it has exhibited higher activity than the parent zeolite.

Keywords Beta zeolite · Characterization · Aluminium sites · Acidity · Methanol transformation

1 Introduction

Beta zeolites have demonstrated to be very efficient catalysts for a great variety of organic reactions [1]. In order to improve their activity and/or selectivity, they can be modified by following different strategies.

A typical procedure for altering the surface properties of beta zeolites has consisted in their dealumination, which has been carried by several procedures, such as the treatment with either nitric or oxalic acid and the steaming at high temperature [2]. For example, the dealuminated samples exhibited an increased activity in the acylation of naphthalene and 2-methoxynaphthalene with acetic anhydride and in the esterification of benzyl alcohol with hexanoic acid due to the relative increase in the amount of strong acid sites and the enhanced accessibility of the reactants to the active sites, which is caused by removal of extra-framework Al species during the acid treatments [3]. However, these treatments also decreased the population of acid sites of weak and particularly of medium strength and as a consequence decreased the catalytic activity in the hydroisomerization of light paraffins for some Pt supported samples [4]. Also, the marked increase in the number of highly acidic sites favoured cracking. In general, the dealumination affects the local environment of both framework and extra-framework aluminium atoms and so their acid properties [5, 6].

Some studies on the dealumination–realumination processes of different zeolites have also been carried out for controlling their physicochemical properties [7, 8]. Thus, beta zeolites were easily dealuminated by HCl treatment and later the Al species in the solution were reinserted into the framework by adjusting the pH value of the suspension. However, the catalytic activity of the realuminated samples in the cumene cracking, which is catalysed by Brönsted acid sites, generally decreased compared to the parent zeolite. By contrast, the treatment with a $NaAlO_2$ aqueous solution increased the number of both Brönsted and Lewis acid sites and slightly improved the catalytic activity in the disproportionation and transalkylation of toluene and C_9 aromatics [9]. Also, the distribution of aluminium in beta zeolite has been investigated for a sample which was dealuminated by treatment with HCl and realuminated by

D. Esquivel · A. J. Cruz-Cabeza · C. Jiménez-Sanchidrián · F. J. Romero-Salguero (✉)
Department of Organic Chemistry, Faculty of Sciences, Córdoba University Research Institute for Fine Chemistry and Nanochemistry (IUIQFN), Campus de Rabanales, Edificio Marie Curie, Ctra. Nnal. IV, km 396, 14014 Córdoba, Spain
e-mail: qo2rosaf@uco.es

Present Address:
A. J. Cruz-Cabeza
Universiteit van Amsterdam, Van't Hoff Institute for Molecular Science, Science Park 904, 1098 XH Amsterdam, The Netherlands

reaction with aluminium isopropoxide [10], although no catalytic activity was provided.

The acid-basic properties of beta zeolites can be also modified by the incorporation of different metal ions. Thus, the impregnation with cerium, iron and tungsten, among others, has demonstrated to improve its catalytic performance in the benzylation of benzene and toluene with benzyl alcohol in the liquid phase due to their increased acidity [11]. The concentration of weak Brönsted acid sites increases in La^{3+} exchanged beta zeolite [12], which exhibits a high activity in several reactions, e.g. the transesterification of triglycerides with methanol [13].

Herein, we report the modification of the protonic form of a beta zeolite with aluminium ions. The structural and surface properties of the so treated zeolite have been studied by using several techniques and they have been related to its performance in a model reaction, i.e., the transformation of methanol into hydrocarbons as a model reaction. Although some of its mechanistic aspects remain controversial, particularly the formation of the first carbon–carbon bond, this reaction has been proposed as a test reaction for different molecular sieves [14, 15]. The hydrocarbon pool mechanism is generally accepted for explaining the transformation of methanol into hydrocarbons [16]. Brönsted acid sites are essential to enhance the catalytic activity for this reaction.

2 Experimental

A NH_4-β zeolite with a Si/Al ratio of 12.5, purchased from Zeolyst Int. (ref. CP814E), was calcined at 600 °C for 3 h to obtain its protonic form, H-β. The aluminium-modified zeolite was prepared under typical conditions for ion-exchange, i.e., by stirring a suspension of the zeolite in a 0.3 M $Al(NO_3)_3{\cdot}9H_2O$ aqueous solution at 80 °C during 24 h and using approximately 6 mL of liquid per gram of solid. After filtration and washing it was calcined at 600 °C for 3 h, thus giving Al-β.

X-Ray powder diffraction (XRD) patterns were recorded on a Siemens D-5000 powder diffractometer (Cu-Kα radiation). Crystallinity was calculated by comparison of the peak areas at $2\theta = 22.5$ of the modified zeolite with that of the acidic β zeolite and the average crystal size by using the Scherrer equation. Elemental compositions were determined by energy dispersive X-ray analysis (EDAX) on a Jeol JSM-5400 instrument equipped with a Link ISI analyser and a Pentafet detector (Oxford). ^{27}Al MAS NMR spectra were recorded at room temperature in a Bruker Avance-400 WB spectrometer (9.4 T) at a spin rate of 12 kHz. A resonance frequency of 104.2 MHz, pulse of 10°, a recycle delay of 0.5 s and a number of scans of 6000 were applied. Chemical shifts were measured relative to $Al(H_2O)_6^{3+}$ (0 ppm). XPS spectra were recorded with a SPECS Phoibos HAS 3500 150 MCD. The residual pressure in the analysis chamber was 5×10^{-9} Pa. Accurate binding energies (BE) have been determined with respect to the position of the Si 2p peak at 103.4 eV. The peaks were decomposed using a least-squares fitting routine (Casa XPS software) with a Gauss/Lorenz ratio of 70:30 and after subtraction of a linear background. The surface atomic concentration ratios were calculated using sensitivity factors from the Casa XPS element library. N_2 isotherms were determined on a Micromeritics ASAP 2010 analyzer at −196 °C. Temperature programmed desorptions of pyridine and acetonitrile were carried out by injecting several pulses of 1 μL till saturation of the catalyst at 110 °C and 140 °C for acetonitrile and pyridine, respectively. After 12 h in a N_2 flow, desorption was carried out at a rate of 5 °C min^{-1} up to 650 °C.

Catalytic reactions were carried out at 400 °C in a microanalytical pulse reactor. Ten milligrams of catalyst were held by small plugs of glass wool in the 4 mm-diameter reactor tube. Helium was used as carrier gas at a flow rate of 100 mL min^{-1}. A pulse size of 0.2 μL was set. The analyses were performed on a Petrocol 100 m × 0.25 mm ID capillary column and the identity of each reaction product was determined by mass spectrometry using a Hewlett Packard 5971A mass selective detector. No variation in the product composition was observed after five consecutive pulses. Although the pulse reactor has been shown to be of limited usefulness with respect to mechanistic studies, it provides a simple basis for the rapid screening of different catalysts [17]. In addition, this technique minimizes the effect of the coke deposition [18]. Also, the configuration of the system avoids the condensation of heavy aromatic products in the transmission lines.

3 Results and Discussion

The XRD pattern of the Al-modified zeolite (Fig. 1) revealed that the original structure was preserved but with a small loss of crystallinity (Table 1). No peaks other than those corresponding to the β zeolite were detected. However, the Si/Al ratio for the H-β sample was slightly lower than that for the Al-β zeolite presumably due to the acidic conditions provided by the aluminium ions ($pK_a = 5.0$) which promoted a slight dealumination. Consequently, Al ions from the solution seemed not to be incorporated into the zeolite by ion exchange.

Both zeolites, H-β and Al-β, exhibited a combined type I and IV isotherm adsorption behavior due to the presence of zeolitic micropores as well as mesopores formed by the aggregation of crystals (Fig. 2). No new mesoporosity was generated after the aluminium treatment. The Al-β sample

experienced small losses in surface area, micro and mesopore volumes compared to the H-β sample (Table 1).

^{27}Al MAS NMR spectra of zeolites H-β and Al-β are shown in Fig. 3. The protonic zeolite showed two peaks with chemical shift values of approximately 55 and 0 ppm, which were assigned to framework tetrahedral and partially hydrolyzed octahedral aluminium species, respectively [19]. Also, a broad signal at 30–35 ppm had been attributed to the third aluminium species, that is, pentacoordinated aluminium (Al^{V}) and/or Al atoms in highly distorted tetrahedral coordination [20, 21]. In addition, a shoulder at ca. −12 ppm has been assigned to Al^{VI} in distorted octahedra [22]. When H-β was subjected to ion exchange conditions with Al^{3+} giving rise to Al-β, a decrease of both the octahedral and the third aluminium species was observed. On the contrary, the band corresponding to tetrahedral aluminium was more intense in this case. At the same time, the broad peak centred at ca. −12 ppm remained. These observations suggested a partial reincorporation of the octahedral and third aluminium species to the zeolite framework (tetrahedral coordination). Fajula and col. [23] reported the aluminium reinsertion into tetrahedral sites in beta zeolite upon ion-exchange with ammonium nitrate. However, they demonstrated the reversibility of the dealumination–realumination process after a thermal treatment and so that the octahedral aluminium is restored in the same extension when the exchanged zeolite was calcined to give its protonic form. In our case, the aluminium-modified zeolite exhibited a lower fraction of the octahedral aluminium species than the parent sample both in their protonic forms obtained after calcination.

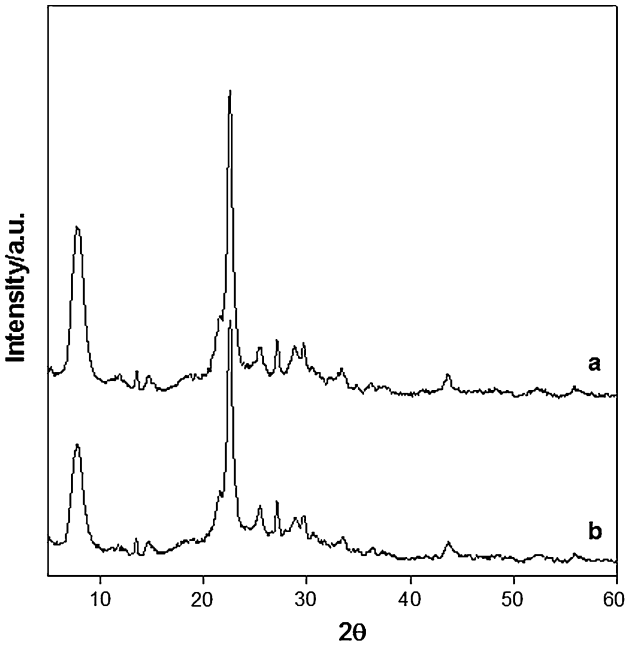

Fig. 1 XRD patterns of H-β (*a*) and Al-β (*b*)

BE of Al 2p levels are given in Table 2. Since they are unable to distinguish between tetrahedral and octahedral aluminium, the modified Auger parameters (α') were calculated. The full width at half-maximum (fwhm) values suggested the existence of different aluminium coordination states. The Al KLL peaks were decomposed into three components whose α' values are reported in Table 3. Both components 1 and 2 could be attributed to Al atoms in

Table 1 Composition and physicochemical properties of H-β and Al-β zeolites

Zeolite	Si/Al bulk ratio	Si/Al surface ratio	Crystallinity (%)	Average crystal size (nm)	Surface area ($m^2\ g^{-1}$)	Mesopore volume ($cm^3\ g^{-1}$)	Micropore volume ($cm^3\ g^{-1}$)
H-β	12.5	11.6	100	67	582	0.89	0.22
Al-β	14.5	13.4	86	53	522	0.85	0.19

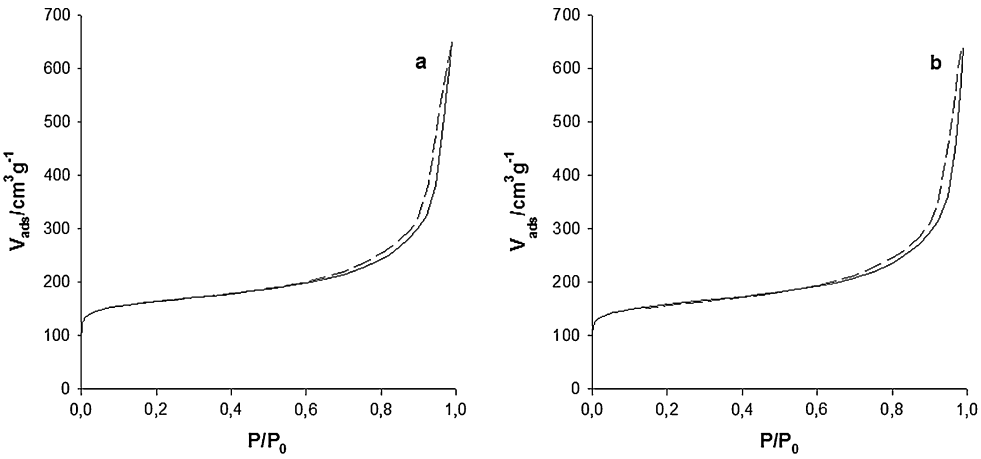

Fig. 2 Nitrogen adsorption–desorption isotherms of H-β (*a*) and Al-β (*b*)

tetrahedral sites whereas component 3 was assigned to octahedrally coordinated aluminium [24]. Thus, the contribution of the octahedral aluminium species was lower in Al-β than in H-β.

The surface acid properties were studied by TPD of two probe molecules, i.e. pyridine and acetonitrile (Fig. 4). As expected, both zeolites exhibited similar profiles since they had essentially the same types of acid sites. However, the small differences in their curves, which have been analyzed by deconvolution, revealed their different distributions of acid sites.

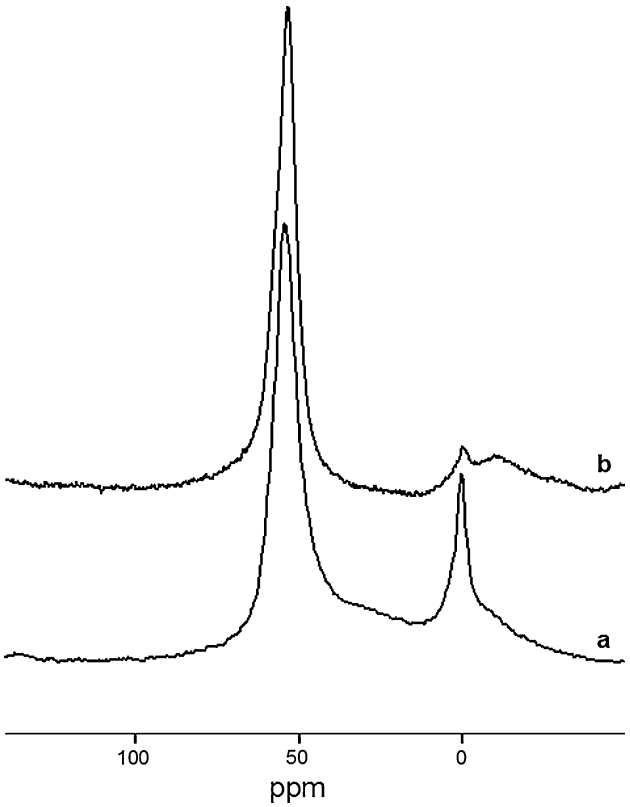

Fig. 3 ^{27}Al MAS NMR spectra at 14 kHz for samples H-β (*a*) and Al-β (*b*)

The experimental pyridine TPD curves were only satisfactorily fitted by using 6 peaks (Fig. 4, left). Those peaks between 200 and 350 °C were considered as weak acid sites, whereas those in the range from 350 to 550 °C and from 550 to 700 °C would correspond to medium and strong acid sites, respectively. The desorption curve for Al-β was very similar to that of H-β except for a slightly higher concentration of centres of medium strength. It was confirmed by a deconvolution analysis of these curves which revealed that the population of weak, medium and strong acid sites were respectively 291, 446 and 173 μmol g^{-1} for H-β and 195, 510 and 145 μmol g^{-1} for Al-β (Table 4). Thus, the aluminium modified sample exhibited a decrease of 33 and 16% in weak and strong sites population, respectively, and an increase of 14% in the amount of medium sites, in accordance with its higher fraction of tetrahedral aluminium.

The acetonitrile TPD curves are depicted in Fig. 4. Both samples gave a peak at low temperature (at ca. 270 °C) attributed to its interaction with Brönsted acid sites and another one at high temperature (above ca. 400 °C) ascribed to its desorption from Lewis acid sites [25]. As expected, the former band was slightly less intense (ca. 6%) for the sample Al-β (Table 5). However, the latter one, which was deconvoluted into three contributions, decreased up to a 46% for the aluminium modified zeolite, in accordance with the reduction in the percentage of component 3 determined by XPS analysis. Clearly, both measurements are related to aluminium atoms in an octahedral coordination.

Table 2 Binding energies (BE, eV) and full width at half-maximum (FWHM, eV) of Al 2p peak and kinetic energy (eV), FWHM (eV) and modified Auger parameter (α', eV) of the Al KLL peak

Zeolite	Al 2p		Al KLL		
	BE	FWHM	KE	FWHM	α'^{a}
H-β	75.2	2.5	1385.5	3.4	1460.6
Al-β	74.9	2.3	1385.7	4.4	1460.6

[a] $\alpha' =$ BE Al 2p + KE Al KLL

Table 3 Kinetic energies (eV), fractions and modified Auger parameter after deconvolution of the Al KLL peaks into three components

Zeolite	Component 1			Component 2			Component 3		
	KE	(%)	α'	KE	(%)	α'	KE	(%)	α'
H-β	1383.3	27	1458.5	1385.7	67	1460.9	1386.8	6	1462.0
Al-β	1383.7	35	1458.6	1385.9	62	1460.8	1386.8	3	1461.7

Both zeolites, H-β and Al-β, were tested as catalysts in the transformation of methanol to hydrocarbons at 400 °C [14, 15]. Below this temperature, the production of hydrocarbons was negligible and the main product was dimethyl ether. At 400 °C, aromatic compounds, in particular hexamethylbenzene and pentamethylbenzene, were the main products of the reaction (Table 6). In addition, alkanes and alkenes (3 to 6 carbon atoms) were also significant. The major compounds in the alkene fraction were propene (ca. 70–90%) and isobutene (ca. 10–30%) although ethylene and 2-methylbutene were also found in small proportions (ca. 5%) and compounds like 2-methylhexenes were observed very rarely and in trace amounts (less than 3% of the total alkenes). Isobutane was the main alkane and contributed with ca. 60% to this fraction. Both Al-β and H-β produced a higher proportion of alkanes than alkenes, being the proportion of isobutane higher than that of isobutene.

The transformation of methanol into hydrocarbons requires the participation of Brönsted acid sites [14, 26]. For instance, the incorporation of metal cations by ion exchange in H-β usually led to a decrease in the catalytic activity [24]. However, the treatment with aluminium cations gave rise to an increase (ca. 8%) in the overall conversion to hydrocarbons (Table 6) in accordance with the enhanced population of medium strength acid sites. The differences in selectivity for both catalysts were also evident. Particularly, the yield to polymethylated aromatic

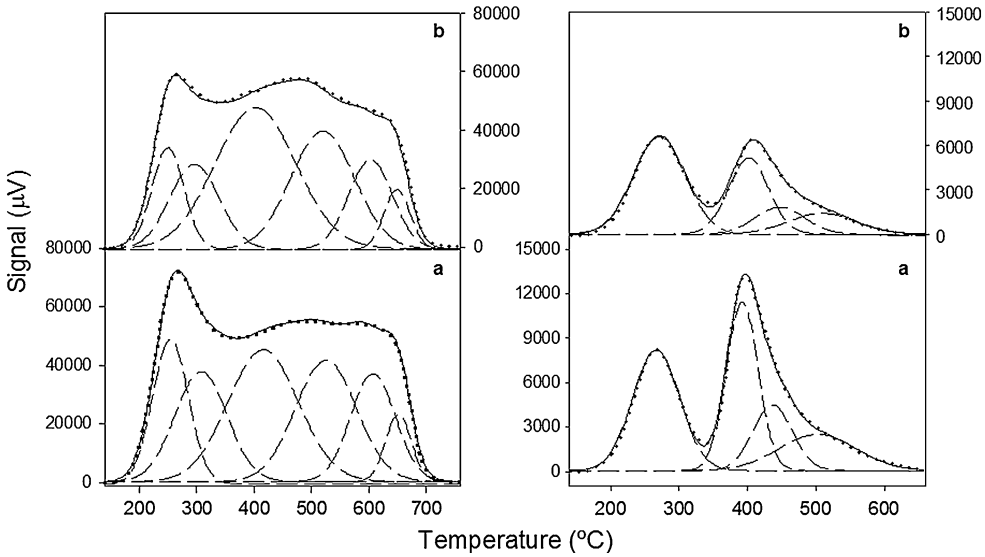

Fig. 4 TPD curves (*solid lines*) of pyridine (*left*) and acetonitrile (*right*) for H-β (*a*) and Al-β (*b*) zeolites showing their deconvolution into several peaks (*dashed lines*) and the resulting calculated desorption (*dotted lines*)

Table 4 Surface acidity of H-β and Al-β zeolites determined by deconvolution of the pyridine TPD curves

Zeolite	$n_{pyridine}$ (mmol g^{-1})	Pyridine desorption X_i (%) (T_i (°C))					
		Peak 1	Peak 2	Peak 3	Peak 4	Peak 5	Peak 6
H-β	0.91	15 (255)	17 (309)	27 (418)	22 (527)	14 (609)	5 (653)
Al-β	0.85	10 (250)	13 (296)	36 (403)	24 (520)	12 (606)	5 (651)

X_i is the percentage population of the i sites

T_i is the temperature in °C of the peak maxima of the i sites

Table 5 Surface acidity of H-β and Al-β zeolites determined by deconvolution of the acetonitrile TPD curves

Zeolite	$n_{acetonitrile}$ (mmol g^{-1})	Acetonitrile desorption X_i (%) (T_i (°C))			
		Peak 1	Peak 2	Peak 3	Peak 4
H-β	0.31	34 (268)	33 (394)	16 (438)	17 (504)
Al-β	0.21	47 (271)	28 (403)	12 (446)	13 (509)

X_i is the percentage population of the i sites

T_i is the temperature in °C of the peak maxima of the i sites

Table 6 Comparison of the product composition (%wt) in the methanol conversion to hydrocarbons over the protonic and the aluminium modified β zeolites at 400 °C

Products	H-β	Al-β
MeOH	6.7	3.6
MeOMe	24.5	22.3
Ethylene	1.0	–
Propene	6.9	4.4
Isobutane	10.3	10.2
C5-C6 alkanes	8.1	6.8
C4-C6 alkenes	1.6	2.0
Tetramethylbenzenes	1.6	2.3
Pentamethylbenzene	13.3	15.2
Hexamethylbenzene	26.0	33.1

compounds was much higher for Al-β (50.6%) than for H-β (40.9%).

The hydrogen transfer index, i.e. HTI = ($\sum$ C4 alkanes)/($\sum$ C4 alkanes + $\sum$ C4 alkenes) × 100, indicates the catalyst's ability to catalyze the disproportionation of alkenes to alkanes and arenes [27]. Although the Lewis acidity caused by the existence of aluminium atoms in octahedral coordination did not seem to have any influence on the methanol conversion to hydrocarbons [14], some of these species might perturb the bridging hydroxyl groups resulting in enhanced proton acidity [6]. Consequently, sample H-β, which had the highest amount of acid sites and the strongest Brönsted acidity, gave the highest HTI (87.0 and 83.9% for H-β and Al-β, respectively).

4 Conclusion

The treatment with a solution containing Al^{3+} cations only produces small changes in most of the structural and surface properties of a beta zeolite. However, it modifies the distribution of aluminium sites and causes a reduction of the octahedrally coordinated aluminium atoms. As a consequence, the amount of strong Lewis acid sites drastically decreases. Concomitantly, the partial reincorporation of octahedral aluminium to tetrahedral sites gives rise to an increase in the population of Brönsted medium acid sites while those of higher strength decrease. As a result, the aluminium treated sample is more active toward the transformation of methanol to hydrocarbons than the unmodified zeolite. Both materials exhibit different product compositions due to their different distribution of acid sites.

Acknowledgments The authors wish to acknowledge funding of this research by Ministerio de Ciencia e Innovación (Project MAT2010-18778), Junta de Andalucía (Project P06-FQM-01741) and Fondos Feder. The technical support and facilities from Córdoba University's SCAI is greatly appreciated. D.E. thanks Ministerio de Educación y Ciencia for a teaching and research fellowship.

References

1. Jansen JC, Creyghton EJ, Njo SL, Van Koningsveld H, Van Bekkum H (1997) Catal Today 38:205
2. Müller M, Harvey G, Prins R (2000) Micropor Mesopor Mater 34:135
3. Srivastava R, Iwasa N, Fujita S-I, Arai M (2009) Catal Lett 130:655
4. Jiménez C, Romero FJ, Roldán R, Marinas JM, Gómez JP (2003) Appl Catal A 249:175
5. Van Bokhoven JA, Koningsberger DC, Kunkeler P, Van Bekkum H, Kentgens APM (2000) J Am Chem Soc 122:12842
6. Jiménez-Sanchidrián C, Romero-Salguero FJ, Ruiz Arrebola JR (2006) In: Somasundaran P, Hubbard A (eds), Encyclopedia of surface and colloid science, 2nd ed, Taylor & Francis, New York, pp 1143–1168
7. Oumi Y, Mizuno R, Azuma K, Nawata S, Fukushima T, Uozumi T, Sano T (2001) Micropor Mesopor Mater 49:103
8. Oumi Y, Nemoto S, Nawata S, Fukushima T, Teranishi T, Sano T (2002) Mater Chem Phys 78:551
9. Zaiku X, Jiaqing B, Yiqing Y, Qingling C, Chengfang Z (2002) J Catal 205:58
10. Omegna A, Vasic M, Van Bokhoven JA, Pirngruber G, Prins R (2004) Phys Chem Chem Phys 6:447
11. Narender N, Krishna Mohan KVV, Kulkarni SJ, Ajit Kumar Reddy I (2006) Catal Commun 7:583
12. Guzman A, Zuazo I, Feller A, Olindo R, Sievers C, Lercher JA (2005) Micropor Mesopor Mater 83:309
13. Shu Q, Yang B, Yuan H, Qing S, Zhu G (2007) Catal Commun 8:2159
14. Dimitrova R, Gunduz G, Dimitrov L, Tsoncheva T, Yialmaz S, Urquieta-Gonzalez EA (2004) J Mol Catal A 214:265
15. Zenonos C, Sankar G, García-Martínez J, Aliev A, Beale AM (2003) Catal Lett 86:279
16. Haw JF (2002) Phys Chem Chem Phys 4:5431
17. Hutchings GJ, Lee DF, Lynch M (1993) Appl Catal A 106:115
18. Itoh H, Hattori T, Murakami Y (1982) Appl Catal 2:19
19. Pérez-Pariente J, Sanz J, Fornés V, Corma A (1990) J Catal 124:217
20. Samoson A, Lippmaa E, Engelhardt G, Lohse U, Jerschkewitz HG (1987) Chem Phys Lett 134:589
21. Sanz J, Fornés V, Corma A (1988) J Chem Soc. Faraday Trans 1 84:3113
22. Camblor MA, Corma A, Valencia S (1998) J Mater Chem 8:2137
23. Bourgeat-Lami E, Massiani P, Di Renzo F, Fajula F, Des Courieres T (1990) Catal Lett 5:265
24. Esquivel D, Cruz-Cabeza AJ, Jiménez-Sanchidrián C, Romero-Salguero FJ (2011) Micropor Mesopor Mater 142:672
25. Haw JF, Hall MB (1994) J Am Chem Soc 116:7308
26. Sarkadi-Pribóczki É, Kumar N, Salmi T, Kovács Z, Murzin DY (2004) Catal Lett 1–2:101
27. Mikkelsen O, Kolboe S (1999) Micropor Mesopor Mater 29:173